Fluorescence and Photodissociation of Rhodamine 575 Cations in a Quadrupole Ion Trap

Nicholas A. Sassin, Stephanie C. Everhart, Beni B. Dangi, Kent M. Ervin, and Joseph I. Cline

Department of Chemistry and Chemical Physics Program, University of Nevada, Reno, Reno, Nevada, USA

The fluorescence and photodissociation of rhodamine 575 cations confined to a quadrupole ion trap are observed during laser irradiation at 488 nm. The kinetics of photodissociation is measured by time-dependent mass spectra and time-dependent fluorescence. The rhodamine ion signal and fluorescence decay are studied as functions of buffer gas pressure, laser fluence, and irradiation time. The decay rates of the ions in the mass spectra agree with decay rates of the fluorescence. Some of the fragment ions also fluoresce and further dissociate. The photodissociation rate is found to depend on the incident laser fluence and buffer gas pressure. The implications of rapid absorption/fluorescence cycling for photodissociation of dye-labeled biomolecular ions under continuous irradiation are discussed. (J Am Soc Mass Spectrom 2009, 20, 96–104) © 2009 Published by Elsevier Inc. on behalf of American Society for Mass Spectrometry

As an alternative to collision-induced dissociation, surface-induced dissociation, infrared multiphoton dissociation, or direct UV/visible dissociation of biomolecular ions, there has been interest in labeling biomolecules with a chromophore tag to enhance photoactivation efficiency and selectivity. For example, Brodbelt and colleagues studied photodissociation mass spectra to sequence peptides labeled with both infrared absorbers [1] and UV chromophores [2]. Fluorophore labeling is also used in fluorescence resonant energy transfer (FRET) experiments, in which the acceptor/donor interactions of two attached fluorophores depend on the distances between them and therefore can provide conformational information [3–6]. In gas-phase work, Parks and coworkers [7–10] and Zenobi and coworkers [11, 12] investigated the fluorescence of trapped molecular ions commonly used as fluorescent molecular probes of biomolecules. Both groups attached fluorescent probes to peptide cations for the purposes of investigating gas-phase FRET [8, 11].

Chromophore and fluorophore labeling experiments both rely on energy transfer from the absorbing moiety to another part of the biomolecule, either via intramolecular vibrational energy transfer or via radiative or electronic interactions. To understand the initial absorption process and the efficiency of photoactivation, it is of interest to investigate the photophysics and chemical dynamics of the absorption, fluorescence, and dissociation processes in the fluorescent dye molecules themselves in the gas phase. This work investigates the competition between fluorescence and photodissociation of rhodamine dye cations in a quadrupole ion trap. The ion trap is an ideal device for measuring chemical reactions that have slow reaction rates or processes that have long-lived intermediate states because of its ability to store a population of thermalized ions in the same location for extended periods of time. The photodepletion rate of the rhodamine cations is determined here by two independent methods: by directly observing the fluorescence photons and by recording the ion mass spectra. The resulting decays obtained by both methods are compared as a function of pressure, laser fluence, and irradiation time. The mechanism of rhodamine cation photodissociation at 488 nm is discussed.

Several other groups have directly measured fluorescence from ions in various traps [7, 11, 13–16]. Zenobi et al. [11] reported observation of gas-phase FRET using several classes of fluorescent dyes inside an ion cyclotron resonance trap. Danell et al. [8] reported FRET experiments with a pulsed laser system on dye-labeled nucleotides in a quadrupole ion trap.

In previous work [17] we reported the photodissociation kinetics of rhodamine ions held in a quadrupole ion trap and irradiated continuously at 514 nm. Photodissociation decay rates of the parent cation were as slow as 1 s^{-1} and showed a dependence on buffer gas pressure greater than first-order. To explain the slow photodissociation and inefficient collisional stabilization, we postulated that the ions undergo many rapid absorption/fluorescence cycles. Absorbed energy is stored in intermediates either by slow buildup of vibrational energy arising from nonvertical photoabsorption

Address reprint requests to Dr. Joseph I. Cline or Dr. Kent M. Ervin, University of Nevada, Reno, Department of Chemistry/MS 216, 1664 N. Virginia St., Reno, NV 89557-0216. E-mail: cline@unr.edu or ervin@unr.edu

1044-0305/09/$32.00
doi:10.1016/j.jasms.2008.09.009

Published online September 18, 2008
Received July 16, 2008
Revised September 5, 2008
Accepted September 5, 2008

or by infrequent nonradiative transitions (e.g., intersystem crossing) to an intermediate electronic state on the path to photodissociation that is inefficiently collisionally relaxed. Either mechanism could explain the observed inefficient deactivation of the intermediate by helium collisions [17]. In this work, we examine the first hypothesis of rapid absorption and fluorescence cycling by directly observing fluorescence from the trapped ions. We measure the pressure and power dependence of the fluorescence decay rates and compare them with the ion photodissociation kinetics.

Experimental

Rhodamine 575 cations were used exclusively for the fluorescence and photodissociation experiments. The rhodamine 575 (Exciton, Dayton, OH, USA) solutions prepared for the electrospray ionization source were 20 μM in a methanol:deionized water solvent (1:1 by volume). The analyte and solvents were used as supplied without further purification.

All photodissociation and fluorescence processes take place within the confines of a three-dimensional quadrupole ion trap (QIT), also known as a Paul trap. The quadrupole ion trap/time-of-flight (TOF) mass spectrometer [Jordan TOF Products (formerly R. M. Jordan Co.), Grass Valley, CA, USA] with a custom electrospray ionization source has been described previously [17], so the following description is brief. Rhodamine 575 cations formed in the electrospray ionization region are focused into the QIT by a series of ion optics. The ions are trapped inside an "ideal" geometry [18] QIT by a radiofrequency field (983 kHz) where they are irradiated by a laser beam that is normal to the ion beam axis. When collecting fluorescence, the photons emanating from one aperture of the ring electrode of the QIT are counted while the ions are irradiated. At the end of the variable irradiation period, the ions are accelerated out of the trap by a pulsed voltage, 10 μs in width and 500 V in amplitude, applied to one of the end cap electrodes of the QIT. Ions present in the trap at the time of the pulse are extracted into a reflectron TOF mass analyzer. A multichannel plate detects the ions at the end of the reflectron TOF and passes the signal through a preamplifier (gain = 200×). The resulting TOF mass spectrum is processed by a digital storage oscilloscope and computer.

Helium buffer gas is continuously leaked into the trapping volume of the QIT to aid the trapping of the externally created ions. The buffer gas is present in the reaction volume during the entire trapping, fluorescence, and dissociation process. The pressure is measured by an ionization gauge on the vacuum chamber and calibrated as described previously, with estimated uncertainties of 50% for the absolute pressures and within 10% for relative pressures [17]. Parent rhodamine 575 monocations (415 m/z) are the predominant species present in the trap before irradiation. Other ions were below 150 m/z and constituted 10% or less of the trapped ions, based on integrated peak intensities, depending on ion source conditions.

A continuous-wave argon ion laser provides the incident laser light [17]. The laser beam passes through a spatial filter to select a single transverse mode and is focused (f = 1 m) into the vacuum chamber through an antireflection (AR) coated window. Once inside the chamber the laser beam passes through a series of light-baffling apertures (diameter, 1 mm) and transverses the center of the ion trap through two opposing holes (diameter, 2.36 mm) drilled through the ring electrode of the QIT. Past the trap is another set of apertures 6 mm in diameter and a second AR-coated window. The beam terminates immediately past the second AR-coated window where a power meter is positioned to record the intensity of the laser beam transmitted through the trap. The purpose of the apertures along the laser beam path inside the vacuum chamber and the AR windows is to minimize scattered light. The laser beam waist is about 1-mm diameter and is positioned at the center of the QIT. At the beginning of each experiment, the laser beam alignment is adjusted to maximize throughput power and minimize the scatter of the incident light. The incident light was polarized in the horizontal direction referenced to the detection axis.

Fluorescence photon counting is accomplished using a series of detection optics positioned directly above the ion trap. The photon collection optics system developed for this work is shown in Figure 1. The emitted photons are detected through a third 2.36-mm-diameter aperture drilled into the wall of the ring electrode, along an axis perpendicular to both the ion and incident laser beams. These optics are arranged in a confocal geometry with a 1-mm-diameter pinhole to narrow the depth of focus to a small volume around the center of the trap. A notch filter (Semrock Inc., Rochester, NY, USA) can be tilted at different angles relative to the light path to selectively filter different wavelengths. When using 488-nm incident light, the tilted notch filter has an estimated optical density of 4.7 and filters out the majority of 488 ± 5-nm photons without appreciably attenuating the photon counts at other wavelengths. For 514.5-nm incident light, the notch filter is oriented normal to the light path, has an estimated optical density of 6.6, and blocks 514 ± 8-nm light. A photomultiplier tube (PMT; Model R1463, Hamamatsu Photonics, Hamamatsu, Shizuoka, Japan) rests atop the optics stack 0.53 m from the center of the ion trap inside a refrigerated chamber (Model PC410CE, Products for Research, Inc., Danvers, MA, USA). Thermal noise produced by the cooled (233 K) PMT gives less than 10 dark counts s^{-1}. A photon counter (SR400, Stanford Research Systems, Sunnyvale, CA, USA) counts the photons impinging on the PMT over fixed time intervals.

The collection optics improve the signal-to-noise ratio (SNR) of the fluorescence photon counting by simultaneously selecting the trap volume where fluo-

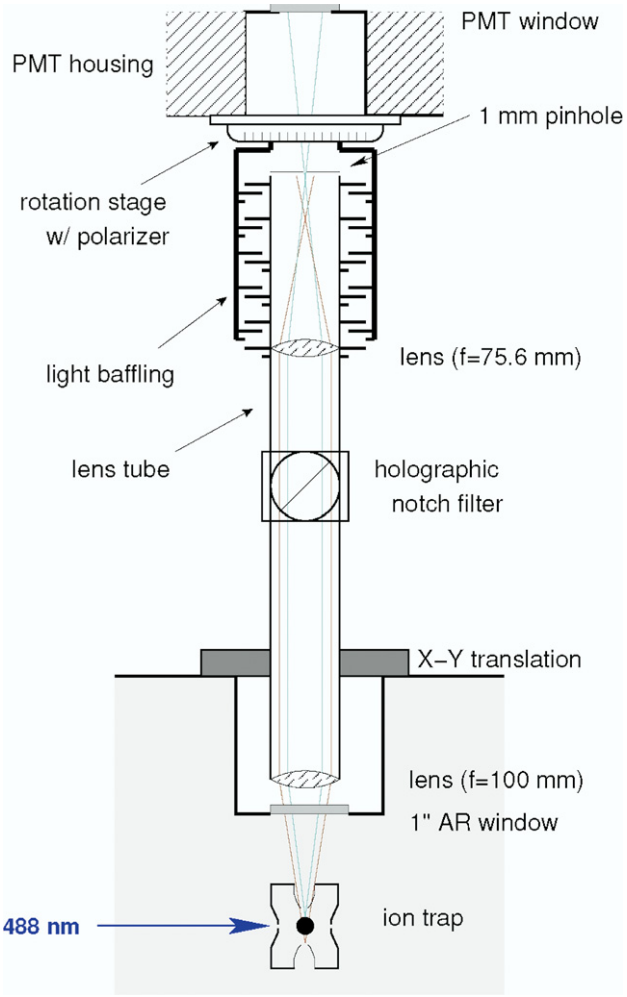

Figure 1. Diagram of the fluorescence collection optics detailing the confocal geometry of the lenses. Light originating at the center of the trap is selectively passed through the 1-mm pinhole.

rescence is most likely to occur, while discriminating against the transmission of photons scattered from trap surfaces. The measures taken to attenuate scattered light along the incident and detection optical paths reduced the background photon counts, without ions in the trap, to 100 counts s^{-1} with 488-nm light at 10 mW. The background count rate using 514-nm incident irradiation is lower: 20 counts s^{-1} at the same power.

The photon detection efficiency is limited by the size of the aperture in the ring electrode, the transmission through the detection optics, and the sensitivity of the PMT. Of these photon-loss mechanisms, the main hindrance limiting the fluorescence signal intensity is the small solid angle in which photons are detected ($\Omega/4\pi = 2.2 \times 10^{-3}$), defined by the diameter of the aperture in the ring electrode. The detection efficiency of the photocathode is roughly 0.14, according to the manufacturer's specifications. The estimated transmission efficiency through the detection optics is 0.59. These values give a total photon detection efficiency of roughly 2.7×10^{-4}, which may be used to estimate a quantum yield of the photons emitted per ion.

The position where the confocal detection optics and the PMT were mounted was optimized visually by focusing on the reflection of laser light off the tip of a metal tube inserted into the center of the trap. Once the depth of field of the detection optics stack was focused, the fluorescence signal intensity was optimized by systematically translating the entire optics stack across a plane over the aperture in the ring electrode.

Data were collected by one of two methods: photon counting or mass spectrometric ion detection. In both modes of operation the period when ions are entering and filling the trap is set at a constant value and controlled by an ion gate. Following the trap filling, a 0.2-s period of time is used to thermalize the kinetic and internal energies of the ions inside the trap to form an ion cloud at the center of the trap. The ions are then irradiated by light from the argon ion laser for a variable irradiation period, which is controlled by a beam shutter (SH05, Thorlabs, Newton, NJ, USA). Immediately following the irradiation period, an extraction pulse transfers the ion cloud into the TOF mass spectrometer. The rhodamine 575 cation peak is then integrated to obtain the irradiation time-dependent data. During the collection of the ion signal, the fill time is a constant 0.75 s and the irradiation time varies between 0 and 4 s. For the fluorescence measurements, we use a fill time of 5 s to increase the number of ions trapped and enhance the fluorescence. The irradiation time during fluorescence measurements was set to 60 s and photons are counted in either 0.5- or 1-s intervals throughout the irradiation period. The irradiation time was extended to longer times than used for the ion data collection to allow longer photon counting times. The fluorescence signal is determined by subtracting the photon counts when no ions are in the trap (scatter) from the photon counts when ions are trapped (fluorescence + scatter). The result of this mode of operation is fluorescence intensity versus time data.

The ion fill time duration linearly coincides with the number of ions present in the trap, at least when operating far from the trap capacity, and partly determines the ion cloud size. Experiments and simulations [19–22] of trapped ion clouds have shown that the axial dimension of the cloud is about 1 mm and the radial dimension of the ion cloud is 2–4 mm under typical operating conditions. Because only a fraction of the ion cloud is thought to be irradiated at any one time by the laser beam (waist, 1 mm) and the ions are continuously moving into and out of the laser beam, the photodissociation rate will be affected by the relative time the ions spend inside and outside of the laser beam. Parks and colleagues [7] investigated the dependence of the fluorescence of trapped ions on the interaction volume, where the ions and laser beam overlap, and found that the photodissociation depends on the interaction volume, the irradiation time, and the laser intensity. Using their reported values, we expect a linear dependence on the fluorescence with the effective overlap of the laser with the ion cloud at constant trap parameter $q_z = 0.24$,

which remains constant for all experiments. Ions absorb photons during passes through the laser beam. The secular frequency of the rhodamine ions in the quadrupole trap is about 85 kHz under the current conditions, giving an oscillation period of 12 μs. This implies that even ions with relatively high kinetic energies, thus orbiting beyond the laser beam waist, would frequently pass through the laser field on the timescale of the experiments. Collisions with the buffer gas thermalize the ion kinetic energies and randomize the ion trajectories. At the pressures used, the average times between collisions range from 184 μs (0.32 mTorr) to 61 μs (0.95 mTorr)—i.e., collisions are also frequent on the timescale of the experiments.

Results and Discussion

The fluorescence signal was found to depend on the intensity and the wavelength of the incident light for three available wavelengths: the 488-, 496-, and 514-nm lines of the argon ion laser. The relative fluorescence count rates normalized by the ion detector signal intensity (mV) and the laser power (W) were found to be 152 ± 13 s^{-1} W^{-1} mV^{-1} at 488 nm, 132 ± 9 s^{-1} W^{-1} mV^{-1} at 496 nm, and 12 ± 3 s^{-1} W^{-1} mV^{-1} at 514 nm. The uncertainties are 95% confidence intervals from four experiments performed on different days, each averaged over 50 fills of the ion trap. The stronger fluorescence at 488 nm is presumably attributed to a greater absorption cross section at that wavelength. Neither the small differences in the range of wavelengths filtered out by the notch filter at 488 and 514 nm (±5 and ±8, respectively) nor the PMT wavelength dependence is accounted for in this analysis. The absorption maximum (λ_{max}) for rhodamine 575 in solution is reported by the manufacturer to be at 518 nm and is expected to blue shift in vacuum. Xanthene dyes have strong absorption blue shifts (~30 nm) in vacuum [7, 11]. Fluorescence measurements at 476-nm incident laser light were attempted, but not observed, because of the poor SNR caused by the low optical density of the notch filter below 488 nm. Because fluorescence is found to be weak at the 514-nm laser line we switched to 488 nm for this work as opposed to the 514-nm laser line used in our previous photodissociation study [17].

Figure 2 shows the dependence of the fluorescence signal on laser power. At low powers, the fluorescence signal increases with laser power in a linear manner. At higher powers, the energy absorbed can no longer be dissipated by radiative or collisional relaxation before dissociation occurs and the fluorescence signal plateaus. The power at which the fluorescence counts are greatest depends on the buffer gas pressure, indicating that collisional relaxation occurs on timescales commensurate with the optical pumping; that is, these results show a competition between the optical pumping rate and relaxation rates. Using an upper-limit estimate of 500 ions in the trap during the photon counting experiment, the calculated transmission efficiency, and the peak fluorescence counts in Figure 2, the maximum fluorescence rate is estimated to be 550 photons ion^{-1} s^{-1} at 0.32 mTorr and 2220 photons ion^{-1} s^{-1} at 0.95 mTorr for absorption of 488-nm incident radiation. For comparison, over the laser power range in Figure 2, the expected absorption pumping rate, calculated using typical solution-phase absorption cross sections (σ) for strong organic dyes of (1–2) × 10^{-16} cm^2 [23], is σI = (1–20) × 10^3 photons s^{-1}, where I is the laser fluence (photons cm^{-2} s^{-1}) for the range of powers used.

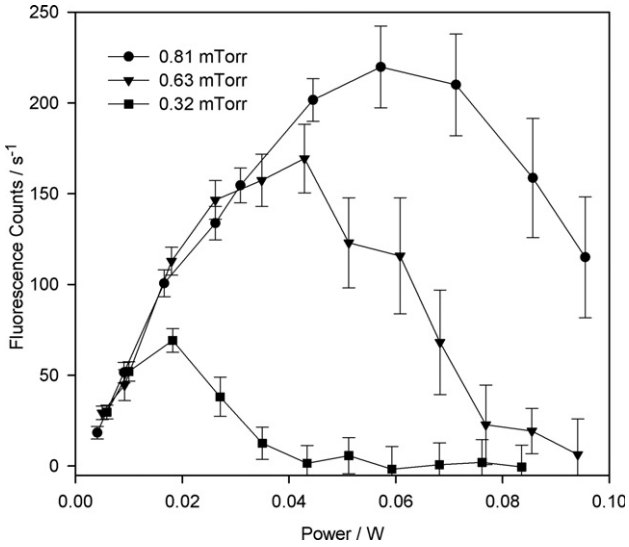

Figure 2. The fluorescence dependence on incident laser power at several helium buffer gas pressures. Fluorescence is measured for 0.5-s time intervals over a total period of 5 s using 488-nm incident irradiation.

An alternative explanation for the power maximum of fluorescence photon counts would be if the incident light saturates the ion cloud. The saturation intensity (I_s) for this organic dye molecule can be approximated by using the expression: $I_s = (h\nu)/(\tau_{eff}\ \sigma)$, where $h\nu$ is the energy of the 488-nm photons, τ_{eff} is the effective fluorescence lifetime, and σ is the absorption cross section [23]. Using $h\nu = 4.07 \times 10^{-19}$ J, $\tau_{eff} = 3 \times 10^{-9}$ s, and the typical absorption cross section for an organic dye molecule like rhodamine, the saturation intensity is calculated to be about 1 MW/cm^2. Even at the highest laser power (0.3 W) implemented in this experiment, the laser intensity (38 W/cm^2) does not approach levels required for saturation. Furthermore, saturation would result in a plateau and not a decrease with increasing powers. Consistent with our previous work monitoring the photodecay of ions at 514 nm [17], we attribute the fluorescence decay mechanism observed here to photodissociation of rhodamine.

The fluorescence decay was found to depend on the irradiation time, buffer gas pressure, and laser fluence. The four plots in Figure 3 display the decay of the fluorescence counts as a function of irradiation time with 488-nm light at various laser intensities and buffer

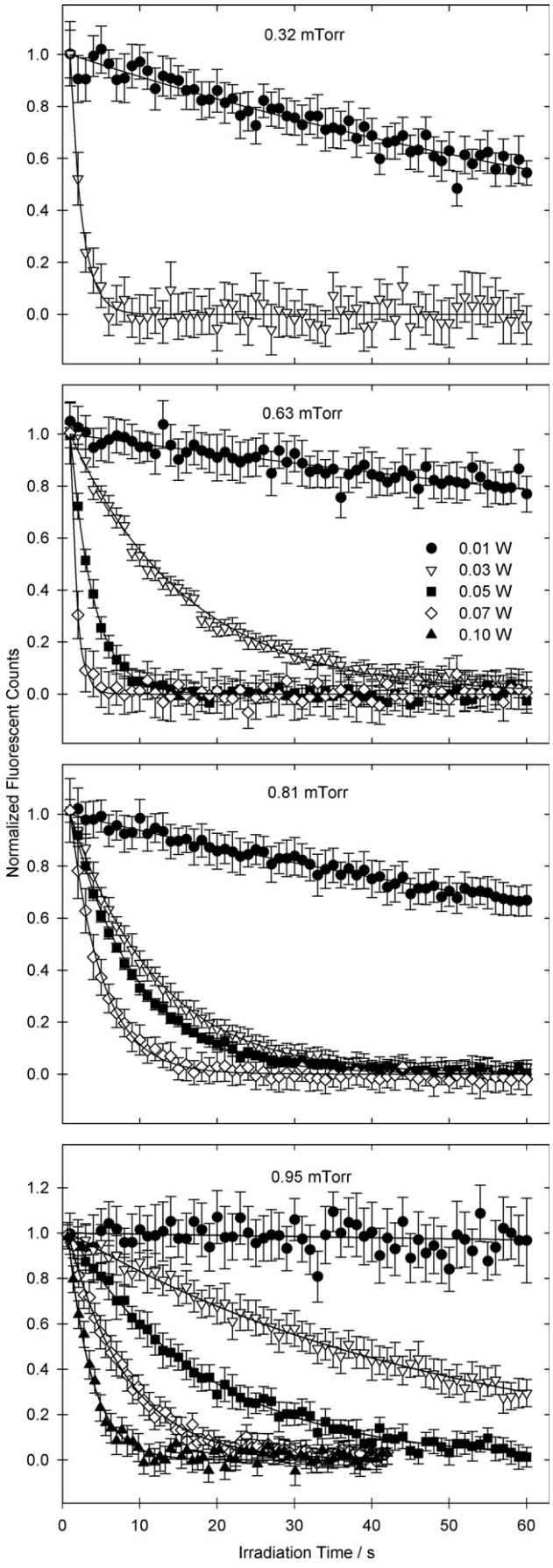

gas pressures. Higher incident laser powers result in faster decay of the fluorescence laser signal. A comparison between the 0.03 W curve on the 0.32 and 0.95 mTorr plots demonstrates the strong pressure dependence. At this power the lowest pressure shows almost complete fluorescence decay after 5 s, whereas about 30% of the fluorescence signal remains after 60 s when using the highest buffer gas pressure.

Each combination of pressure and incident laser power can be fit to an exponential decay to obtain a pseudo-first-order rate constant. The results of fitting the raw data to an exponential decay are presented in Figure 4a, which summarizes the data in Figure 3 using the fitted rate constants. This summary is useful to discern trends in the decay rates as a function of power and pressure. Most noticeable is the nonlinear dependence on laser power, which suggests a multiphoton activation process. Figure 4a also displays evidence of a power threshold at about 0.01 W, below which the fluorescence counts do not decay over the 60-s irradiation period. This threshold is lower than the previously reported [17] photodissociation threshold of 0.05 W using 514-nm incident irradiation, consistent with the higher absorption cross section at 488 nm used here.

Experiments collecting the ion mass spectra and analyzing the rhodamine 575 ion peak area for the various combinations of pressure, laser power, and irradiation time were performed. The laser powers used were from 0.01 to 0.30 W and the pressure range over which ion data were collected matches the pressures during the photon counting experiments. Results from the mass spectrometry show similar dependences on pressure, power, and laser fluence as those of the fluorescence data. The raw data are not shown but are summarized by fitting the individual ion decay curves to an exponential decay and obtaining the pseudo-first-order rate constants in Figure 4b. The pseudo-first-order rate constants were determined only for the combinations of power and pressure where the dissociation is slow enough to be measured. It is obvious from Figures 3 and 4 that there is a strong dependence on laser power and that the optical excitation process competes with the collisional relaxation with the buffer gas, as seen by the slower dissociation with increasing pressure. The approximate 5- to 15-fold difference in decay rate for only a 6-fold increase in laser intensity indicates that the photon absorption at this wavelength is very efficient and the absorbed energy is rapidly transferred into the reaction channel leading to dissociation.

A direct comparison of the rate constants obtained from fluorescence photon counting (Figure 4a) and mass spectral analysis of the parent ion (Figure 4b) is not possible because of the differences in ion fill time

Figure 3. Normalized fluorescence signal decay as a function of irradiation time for four different buffer gas pressures and multiple powers. Decay arises from the dissociation of trapped rhodamine 575 cations. Lines are exponential fits to the data.

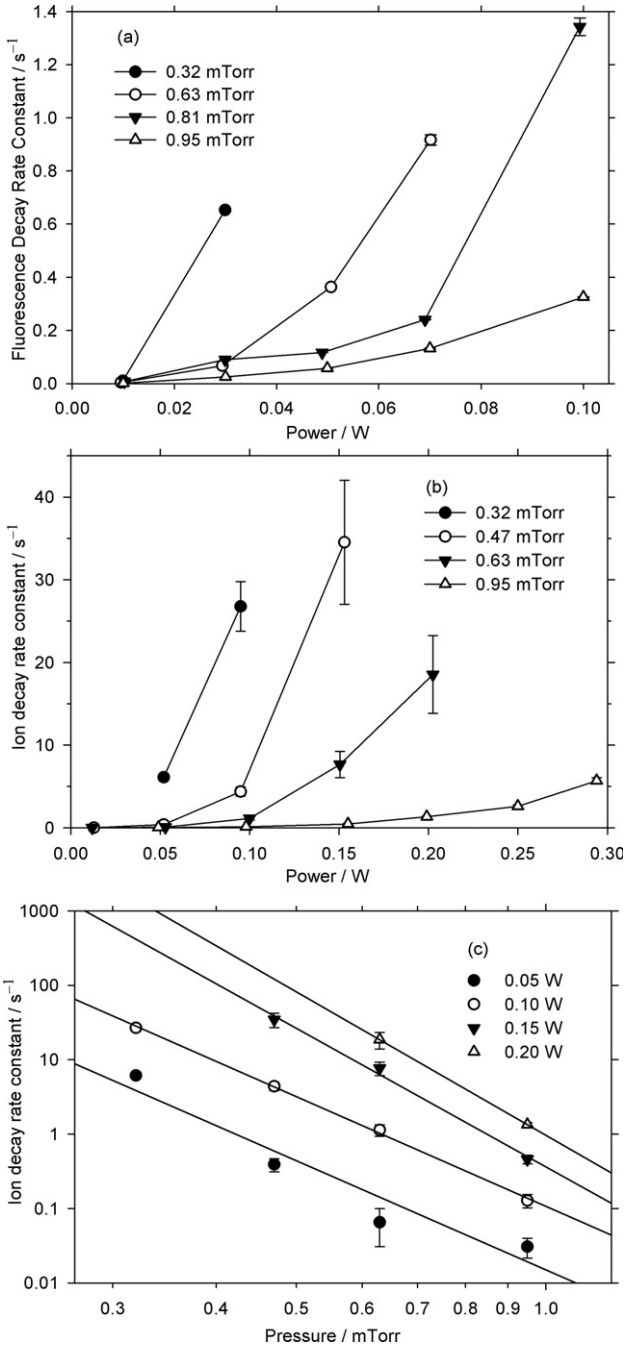

Figure 4. Comparisons of fluorescence and ion decay rates as functions of laser power and pressure. (**a**) Summary of photodissociation data measured by monitoring the fluorescence signal. Symbols are the pseudo-first-order rate constants obtained by fitting the data in Figure 3 to an exponential equation. Lines connect points at the same pressures. The ion trap fill time was 5 s. (**b**) Summary of photodissociation data measured by monitoring the rhodamine 575 cation signal in the mass spectra. Symbols are the pseudo-first-order rate constants obtained by fitting the decay curves of the raw ion data (integrated parent ion intensities) to an exponential equation. Lines connect points at the same pressure. The ion trap fill time was 0.75 s. (**c**) Logarithmic plots of the rhodamine cation decay rate constants from (**b**) versus buffer gas pressure at several laser powers: 0.05 W (solid circles), 0.10 W (open circles), 0.15 W (solid triangles), and 0.20 W (open triangles). Linear regression fits (lines) have slopes of -4.9 ± 0.8 for 0.05 W, -4.9 ± 0.1 for 0.10 W, and -6.2 ± 0.5 for 0.15 W (± 1 standard deviation). The line connecting the two pressures at 0.20 W has a slope of -6.4.

used with each method. We observed a dependence on fill time similar to what Parks et al. [7] reported. Because of differences in detection efficiencies for ions and fluorescence the full range of experimental conditions (power, pressure, and fill time) do not overlap for the two detection methods. However, we compared the two data collection methods under the same experimental conditions, including fill time (3 s) on the same day at a power of 0.05 W and a pressure of 0.37 mTorr. Figure 5a compares the decay of integrated area of the parent ion peak in the collected mass spectra to the fluorescence signal decay and shows a significant deviation. The decay in the signal collected by mass spectrometry is faster than the decay in the photon signal. The slower decay of the fluorescence signal can be explained if some of the fluorescence originates from fragment ions in addition to the parent ions. This possibility was suggested previously in a study on rhodamine 6G in an ion cyclotron resonance trap [11]. The fragment ions that still contain the conjugated electronic structure—and are thus most likely to absorb incident photons—are the cations formed from the loss of

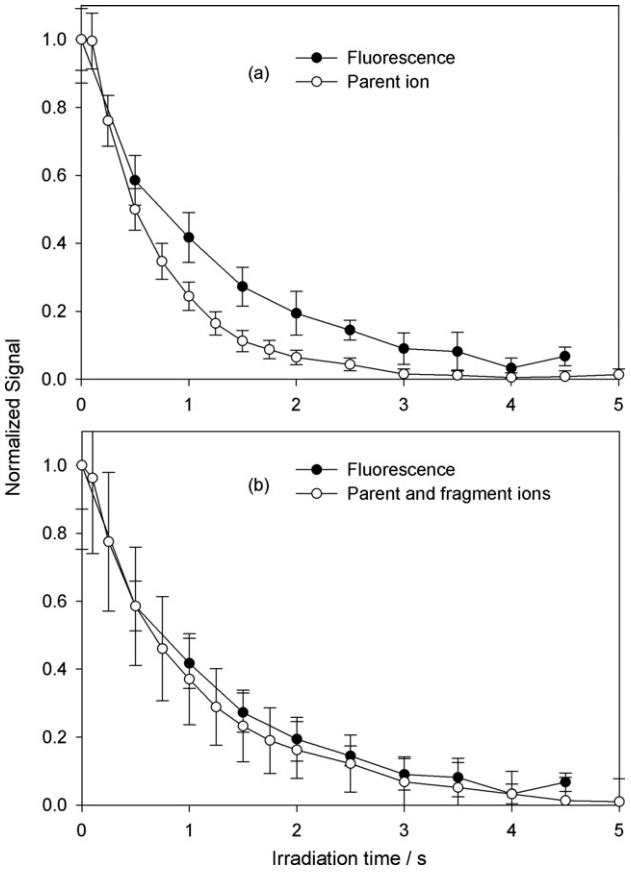

Figure 5. Comparison of data collected by counting emitted photons (solid circles) to mass spectra analysis of ion data (open circles). The top graph (a) shows the fluorescence compared to only the integrated $[R575]^+$ peak. The bottom graph (b) shows fluorescence compared to the integrated area of the $[R575]^+$, $[R575 - Et]^+$, and $[R575 - 2\ Et]^+$ peaks. The ion trap fill time is 3 s during the collection of both fluorescence and ion data.

one or both peripheral ethyl moieties, $[R575 - Et]^+$ and $[R575 - 2\ Et]^+$ at *m/z* 386 and 357, respectively. Both of these fragment cations are evident in the mass spectrum at low irradiation intensities. At longer irradiation times, these fragment ions also decay away; the remaining fragment ions are mostly below *m/z* 200. When the peak areas of the two initial fragments are added to the parent ion area (Figure 5b), the fluorescence and the ion data show good agreement. Additional verification that the slow fluorescence decay is attributed to the fluorescence of fragment ions inside the trap was obtained by isolating the parent ion in the trap by application of a supplemental waveform (stored waveform inverse Fourier transform or SWIFT) [24, 25] to one of the end cap electrodes of the QIT. Fluorescence counts dropped with no apparent decrease in parent ion intensity when the parent ions were isolated.

In an effort to quantify the dependence of the ion signal decay on the buffer gas pressure, Figure 4c shows a log–log plot of the ion decay rate constants for rhodamine 575 cations at several powers versus pressure. The slopes of linear fits to these points yield the power n of the dependence on buffer gas concentration, $k \propto 1/[M]^n$. The results show that the decay rate constants depend inversely on the buffer gas concentration to a high power, $n = 5–6$. This effective order of the reaction is too high for the mechanism to be simple bimolecular ($n = 1$) or termolecular ($n = 2$) collisional deactivation from a photoexcited intermediate. Rather, a more complex multistep mechanism is operative. It is evident that high-order pressure dependence exists, which represents inefficient multistep collisional deactivation of the photoactivated cation.

Photodissociation Mechanism

A nonlinear response in the signal (ion and photon) decay on power often indicates a simultaneous multiphoton event leading directly to the decay of the parent ions. However, simultaneous multiphoton events occur on a timescale that is much faster than the collision frequencies ($1.7 \times 10^4\ s^{-1}$ at 1 mTorr) between the ions and the buffer gas. Thus direct single-photon and simultaneous multiphoton dissociation processes are eliminated here because the data show a distinct pressure dependence. While irradiated, the kinetic energy distribution of the ions is constant and no collisional dissociation is observed under the trapping conditions; therefore the only activation possibility is by absorption of photons. As such the most likely activation pathway at the powers implemented is by multiple sequential photon absorption events. The activation process is highly dependent on the incident laser power used and the photodissociation lifetime varies with the laser intensity. The ion trap is useful for the empirical determination of the activation process by distinguishing between direct photodissociation and an activation process involving several individual excitation steps.

There are two possibilities for deactivation of activated parent ion intermediates. First, collisional deactivation is evidenced by the dependence of the decay rate on buffer gas pressure. The mean collisional period can be estimated from the Langevin–Gioumousis–Stevenson (LGS) [26] collision rate as 58 μs with 1 mTorr helium in the trap. The second deactivation pathway is by fluorescence. Prompt fluorescence processes are expected to have excited-state lifetimes of <5 ns. Because of the pressure dependence of the signal decay and the fact that prompt fluorescence deactivation is expected to occur at least 10,000 times faster than collisions, we hypothesize that there exists a intermediate state, represented in Figure 6 as A^+, that is distinct from the initially excited-state A* from which fluorescence occurs. The A^+ state is a necessary intermediate for photodissociation. Figure 6 depicts the absorption/fluorescence cycle, $A \leftrightarrow A^*$, comprising the majority of transitions taking place in each irradiated rhodamine cation. Occasionally this cycle is interrupted by a transition to the A^+ intermediate state from which the molecule can either absorb additional photons and dissociate or collisionally relax back into the absorption/fluorescence cycle. Among the possible such nonradiative $A^* \rightarrow A^+$ transitions is intersystem crossing from an excited singlet state to a triplet state, internal conversion between singlet states, and vibrational relaxation. Note that Figure 6 depicts a simplified version of the kinetic schemes tested in our previous study [17]. These possibilities cannot be distinguished by the present experiments, but can be assumed to occur based on the slow decay of the rhodamine cations as also observed at 514 nm [17] and the direct observation of fluorescence in this work. The observed high-order pressure dependence is evidently the result of inefficient collisional

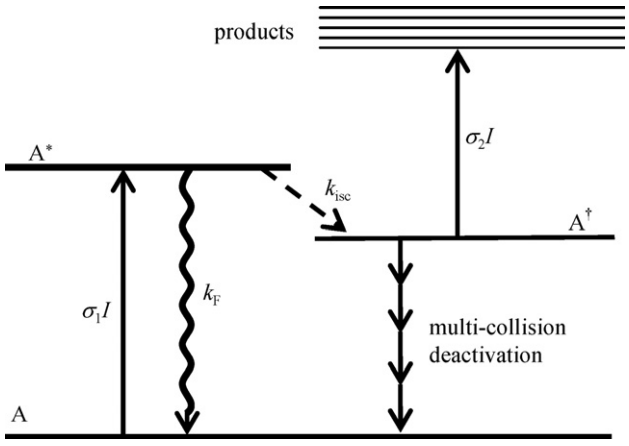

Figure 6. Simplified schematic of the excitation pathway of rhodamine 575 induced by visible light. A absorption of the parent ion to A* is dependent on the absorption cross section, σ_1, and laser fluence, I. The A* fluorescence has the rate constant, k_F. The transition into an intermediate state is depicted by the dotted arrow occurring at an intersystem crossing rate, k_{isc}. Absorption of an additional photon leads to dissociation from the intermediate state, A^+.

deactivation from the putative long-lived A^+ intermediate, which requires multiple collisions to fully dissipate the absorbed energy.

Conclusions

Irradiation of rhodamine 575 cations confined to a small volume inside a quadrupole ion trap induces photodissociation. The decay of the rhodamine cations was measured separately by two distinct methods: by counting emitted photons and by analysis of mass spectra. Comparison of the two methods demonstrates that the extent of dissociation can be monitored by either detection method. It was also shown that a small portion of the photon counts originate from fragments that are also fluorescing. Inclusion of all fluorescing ion peaks in the mass spectra analysis gave identical decay rates to those obtained from the photon counting experiment. The agreement between the two collection methods indicates that they are independent measures of the same photoactivation/deactivation processes taking place inside the trap. In addition, the fluorescence rate is much faster than the dissociation rate under the same laser fluence and pressure conditions, showing that the absorption/fluorescence cycling must occur much faster than the rate-limiting step along the photodissociation pathway, and at a much higher rate than transitions to the intermediate state leading to dissociation. In agreement with our previous report [17], the photodepletion rate was found to depend on the buffer gas pressure and laser fluence, which indicates that optical pumping is in competition with collisional cooling. Proof of the previously hypothesized deactivation pathway was found by detecting the fluorescence.

The observations in this work have clear implications for photoactivation experiments involving biomolecules labeled with visible or UV chromophores. If the chromophore fluoresces efficiently, as is likely the case for strongly absorbing dye labels, radiative deactivation may compete with transfer of energy to the rest of the molecule and with collisional deactivation. That is, the photoactivation process is likely to be more complex than merely single or simultaneous multiple photon absorption leading directly to photodissociation. We have shown here and in our previous study [17] that under continuous radiation conditions, the buildup of energy can occur over long time periods, up to seconds. Generally, lower pressures and higher laser powers are better for ion activation experiments where rapid and extensive fragmentation is desirable. For experiments that rely on fluorescence detection, high buffer gas pressures are desirable to control energy buildup and dissociation of the fluorophore ions.

By measuring the fluorescence as a function of incident laser wavelength, this technique could be used in future experiments to obtain excitation spectra for many organic dye molecules in the gas phase. Rhodamine 575 has been shown to fluoresce without dissociation for extended periods of time at 0.01 W for a typical QIT operation pressure of approximately 1 mTorr and is a good candidate for gas-phase fluorescence probe experiments, including FRET. Another interesting application uses the combination of SWIFT waveform isolation and fluorescence detection. By combining those two techniques to isolate a single ion population at a time, it would be possible to determine the contribution of each ionic species to the total fluorescence.

Acknowledgments

National Science Foundation Grants CHE-0110103 and PHY-0304615 supported this work. We thank Dr. Joel Parks and Dr. Anthony Iavarone for helpful discussions concerning the initial detection of the fluorescence signal. Dr. Wayne Stanbery assisted in the design of the irradiation and detection optics. Walt Weaver performed the machining of the custom housing components used for mounting the detection optics stack.

References

1. Gardner, M. W.; Vasicek, L. A.; Shabbir, S.; Anslyn, E. V.; Brodbelt, J. S. Chromogenic Cross-Linker for the Characterization of Protein Structure by Infrared Multiphoton Dissociation Mass Spectrometry. *Anal. Chem.* **2008,** *80,* 4807–4819.
2. Wilson, J. J.; Brodbelt, J. S. MS/MS Simplification by 355 nm Ultraviolet Photodissociation of Chromophore-Derivatized Peptides in a Quadrupole Ion Trap. *Anal. Chem.* **2007,** *79,* 7883–7892.
3. Scholes, G. D. Long-Range Resonance Energy Transfer in Molecular Systems. *Annu. Rev. Phys. Chem.* **2003,** *54,* 57–87.
4. Jares-Erijman, E. A.; Jovin, T. M. FRET Imaging. *Nat. Biotech.* **2003,** *21,* 1387–1395.
5. Wouters, F. S. The Physics and Biology of Fluorescence Microscopy in the Life Sciences. *Contemp. Phys.* **2006,** *47,* 239–255.
6. Aaron, R. C.; Medintz, I. L.; Mattoussi, H. Förster Resonance Energy Transfer Investigations Using Quantum-Dot Fluorophores. *ChemPhysChem* **2006,** *7,* 47–57.
7. Khoury, J.; Rodriguez-Cruz, S.; Parks, J. Pulsed Fluorescence Measurements of Trapped Molecular Ions with Zero Background Detection. *J. Am. Soc. Mass Spectrom.* **2002,** *13,* 696–708.
8. Danell, A. S.; Parks, J. H. FRET Measurements of Trapped Oligonucleotide Duplexes. *Int. J. Mass Spectrom.* **2003,** *229,* 35–45.
9. Iavarone, A. T.; Parks, J. H. Conformational Change in Unsolvated Trp-Cage Protein Probed by Fluorescence. *J. Am. Chem. Soc.* **2005,** *127,* 8606–8607.
10. Iavarone, A. T.; Meinen, J.; Schulze, S.; Parks, J. H. Fluorescence Probe of Polypeptide Conformational Dynamics in Gas Phase and in Solution. *Int. J. Mass Spectrom.* **2006,** *253,* 172–180.
11. Dashtiev, M.; Azov, V.; Frenkevich, V.; Scharfenberg, L.; Zenobi, R. Clear Evidence of Fluorescence Resonance Energy Transfer in Gas-Phase Ions. *J. Am. Soc. Mass Spectrom.* **2005,** *16,* 1481–1487.
12. Dashiev, M.; Zenobi, R. Effect of Buffer Gas on the Fluorescent Yield of Trapped Gas-Phase Ions. *J. Am. Soc. Mass Spectrom.* **2006,** *17,* 855–858.
13. Peng, W.-P.; Cai, Y.; Lee, Y.; Chang, H.-C. Laser-Induced Fluorescence/Ion Trap as a Detector for Mass Spectrometric Analysis of Nanoparticles. *Int. J. Mass Spectrom.* **2003,** *229,* 67–76.
14. Koczorowski, W.; Szawiola, G.; Walaszyk, A.; Buczed, A.; Stefanska, D.; Stachowska, E. Experimental Investigation of the Stability Diagram for Paul Traps in the Case of Praseodymium Ions. *Hyperfine Interact.* **2006,** *171,* 233–241.
15. Bushev, P.; Rotter, D.; Wilson, A.; Dubin, F.; Becher, C.; Eschner, J.; Blatt, R.; Steixner, V.; Rabl, P.; Zoller, P. Feedback Cooling of Single Trapped Ions. *Phys. Rev. Lett.* **2006,** *96,* 043003/1–043003/4.
16. Wang, Y.; Hendrickson, C. L.; Marshall, A. G. Direct Optical Spectroscopy of Gas-Phase Molecular Ions Trapped and Mass-Selected by Ion Cyclotron Resonance: Laser-Induced Fluorescence Excitation Spectrum of Hexafluorobenzene ($C_6F_6^+$). *Chem. Phys. Lett.* **2001,** *334,* 69–75.
17. Sassin, N.; Everhart, S.; Cline, J.; Ervin, K. Photodissociation and Collisional Cooling of Rhodamine 575 Cations in a Quadrupole Ion Trap. *J. Chem. Phys.* **2008,** *128,* 234–305.
18. Goeringer, D. E.; Viehland, L. A.; Danailov, D. M. Prediction of Collective Characteristics for Ion Ensembles in Quadrupole Ion Traps Without Trajectory Simulations. *J. Am. Soc. Mass Spectrom.* **2006,** *17,* 889–902.
19. Williams, J. D.; Cooks, R. G.; Syka, J. E. P.; Hemberger, P. H.; Nogar, N. S. Determinations of Positions, Velocities, and Kinetic Energies of Resonantly Excited Ions in the Quadrupole Ion Trap Mass Spectrometer by Laser Photodissociation. *J. Am. Soc. Mass Spectrom.* **1993,** *4,* 792–797.

20. Oomens, J.; von Helden, G.; Meiher, G. Experimental Observation of Laser-Induced Coherent Ion Motion in a Quadrupole Trap. *Int. J. Mass Spectrom.* **2002,** *221,* 163–176.
21. Cleven, C. D.; Cooks, R. G.; Garrett, A. W.; Nogar, N. S.; Hemberger, P. H. Radial Distributions and Ejection Times of Molecular Ions in an Ion Trap Mass Spectrometer: A Laser Tomography Study of Effects of Ion Density and Molecular Type. *J. Phys. Chem.* **1996,** *100,* 40–46.
22. Wu, G.; Cooks, R. G.; Ouyang, Z.; Yu, M.; Chappell, W. J.; Plass, W. R. Ion Trajectory Simulation for Electrode Configurations with Arbitrary Geometries. *J. Am. Soc. Mass Spectrom.* **2006,** *17,* 1216–1228.
23. Siegman, A. E. *Lasers;* University Science Books: Mill Valley, CA, 1986.
24. Soni, M. H.; Cooks, R. G. Selective Injection and Isolation of Ions in Quadrupole Ion Trap Mass Spectrometry Using Notched Waveforms Created Using the Inverse Fourier Transform. *Anal. Chem.* **1994,** *66,* 2488–2496.
25. Colorado, A.; Shen, J. X.; Vartanian, V. H.; Brodbelt, J. Use of Infrared Multiphoton Photodissociation with SWIFT for Electrospray Ionization Laser Desorption Applications in a Quadrupole Ion Trap Mass Spectrometer. *Anal. Chem.* **1996,** *68,* 4033–4043.
26. Gioumousis, G.; Stevenson, D. P. Reactions of Gaseous Molecule Ions with Gaseous Molecules. V. Theory. *J. Chem. Phys.* **1958,** *29,* 294–299.